ADVANCED ENERGY MATERIALS
www.advenergymat.de

Nano-Copper-Assisted Immobilization of Sulfur in High-Surface-Area Mesoporous Carbon Cathodes for Room Temperature Na-S Batteries

Shiyou Zheng, Pan Han, Zhuo Han, Peng Li, Huijuan Zhang, and Junhe Yang**

Rechargeable batteries have attracted increasing attention as power technologies for emerging electric vehicles and grid energy storage, which are expected to mitigate the environmental pollution caused by the use of fossil fuels. Although graphite/lithium transition-metal-oxides ($LiCoO_2$, $LiNiO_2$, and $LiMn_2O_4$, etc.) and lithium-ion batteries have been the dominant power sources for portable electronics and are used in hybrid electric vehicles, the limited ore resources of these materials make durative rising price. Most crucially, the limitations of potential energy density of these metal-oxide cathode materials are a main restriction in terms of large-scale applications of batteries, particularly in electric vehicles and hybrid electric vehicles.[1,2] Therefore, it has become urgent to search for alternative energy-storage systems that could complement the existing lithium-ion batteries and that simultaneously have high energy density and long cycle life, in addition to safety and low cost. Alternatively, sodium-sulfur (Na-S) batteries offer low cost, high capacity and high safety, showing great promissing for grid-scale applications.[2] Both Na and S are abundant and nontoxic elementals on the earth, providing larger availability and lower material cost over the conventional lithium-ion batteries.

High temperature (HT) Na-S batteries, which are built with a solid electrolyte of β-Al_2O_3 and operated at a high temperature of above 300 °C, have been developed for commercial utilization in grid energy storage.[3,4] However, the high operation temperature will cause severe safety concerns in pratical applications; in particular, sodium polysulfides are highly corrosive at this high temperature, which can damage the current collector and containor and lead to fire and/or explosion. The corrosion can be reduced or prohibited by applying corrosion-resistant materials in battery construction, which would increase cost and constrain their large-scale applications. One attempt to solve these issues is to reduce the operation temperature. Recently, Lu and co-workers reported the reversible electrochemical performance of Na-S battery at a lower operation temperature of 150 °C as compared with the conventional HT Na-S batteries by empolying a catholyte solvent for S cathode combining with the solid electrolyte of β-Al_2O_3.[5] However, in principle, the corrosive issues of the sodium polysulfides still exist at this modest temperature. Therefore, a desirable solution of safety problems is to develop a room temperature (RT) Na-S batteries.

Due to low ion conductivity of the solid electrolyte and contact problems between electrodes and current collectors, the configuration design of HT Na-S batteries may not be for RT Na-S batteries. Consequently, several attempts have been made to use polymer electrolytes in RT Na-S batteries.[6–8] Unfortunately, poor cycle life and low capacity were displayed. Liquid electrolytes, which have been demonstrated with good ion conductivity and widely used in lithium-ion batteries and even in Li-S batteries,[9–12] are probably suitable for RT Na-S batteries. However, as is well known, metal Na has similar chemical characteristics to Li, the S cathode in RT Na-S batteries will face the same issues observed in Li-S batteries as: i) low active material utilization, ii) poor cycle life, and iii) low Coulumbic efficiency.[13–15] These drawbacks arise mainly from insulating nature of S, dissolution of polysulfide intermediates in liquid electrolytes and large volume change during charge/discharge.[16–19]

Significant advances have been achieved for Li-S batteries in decade years. The strategies include coating S with conductive polymers or carbon materials, infusing S into porous carbon, and employing different organic electrolytes.[20–25] Among these, one of the most attractive strategies is to encapsulate S with a self-supporting and void-containing carbon matrix.[20–22,26,27] Although the approach of carbon matrix supporting S can significantly improve the S utilization and restrain the solubility of lithium polysulfides, especially by infusing S into the micropores of carbon materials, the C/S composite cathodes showed outstanding cycling life even using carbonate electrolytes, but the S loading is limited to around 30% in the C–S composite due to the insulating nature of S_2, Li_2S_2 and Li_2S and the side reaction between high-order polysolfides and electrolyte, which leads to low overall capacity.[21] In order to increase the S loading of the S-based cathode, a high-cost electrolyte with linear and cyclic ethers, such as bis-(trifluoromethane) sulfonimide lithium (LiTFSI) in dimethoxyethane and dioxolane and tetra(ethylene glycol) dimethyl ether, is generally adopted in the Li-S cells.[28–30] Although the use of high-cost ether-based electrolyte in Li-S batteries can increase S loading, it also generates shuttle reaction, reducing the cycle life and Coulumbic efficiency. Recently, transition metal (Co, Ni and Cu etc.) sulfides have been investigated as cathode materials for Li-S batteries and shown fairly stable cycle life, which are attributed to chemical stabilization of S.[31–36] The similar features between Na and Li bring us to consider whether it is possible

Prof. S. Zheng, P. Han, Dr. Z. Han, Dr. P. Li,
Dr. H. Zhang, Prof. J. Yang
School of Materials Science and Engineering
University of Shanghai for Science and Technology
Shanghai 200093, China
E-mail: syzheng@usst.edu.cn; jhyang@usst.edu.cn

DOI: 10.1002/aenm.201400226

 © 2014 WILEY-VCH Verlag GmbH & Co. KGaA, Weinheim

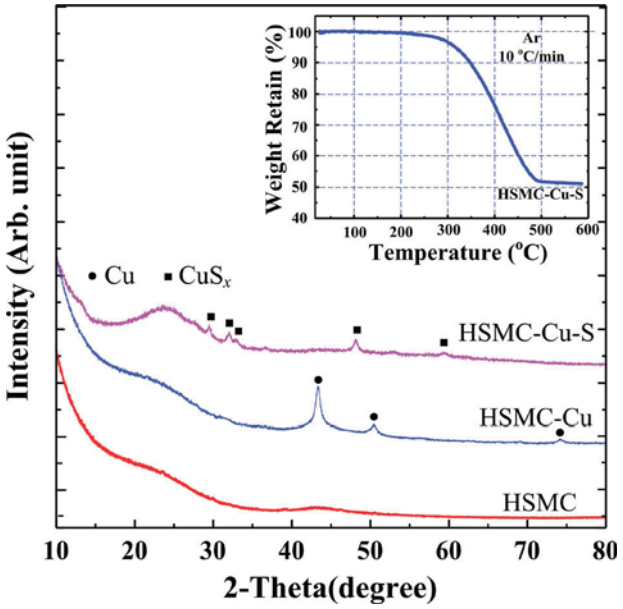

Figure 1. XRD patterns of HSMC, HSMC-Cu, and HSMC-Cu-S. The inset shows the TGA curve for HSMC-Cu-S.

to achieve equally good electrochemical performances for this type S cathode in a RT Na-S battery as in Li-S battery. Here, we report a rational design of nano-copper-assisted immobilizing S in high-surface-area mesoporous carbon (referred to HSMC) cathode with S loading of 50% for RT Na-S batteries. As expected, excellent electrochemical performance is demonstrated. For instance, after 110 cycles, the capacity retention is still as high as 610 mAh g^{-1}. This is the first demonstration of long cycle life cathodes with a relatively high S loading of 50% for RT Na-S batteries.

The phase components and structures of HSMC, HSMC-Cu and HSMC-Cu-S were characterized using X-ray diffraction (XRD), as shown in **Figure 1**. The XRD pattern of the pristine HSMC shows two broad peaks in the range of 20–50°, indicating that HSMC is an amorphous carbon. When Cu is deposited into HSMC using ultrasonic-assisted multiple wetness impregnation and synchrodry techniques, Cu nanoparticles exist in the crystal as demonstrated in the XRD peaks, marked with circles. The followed S impregnation into HSMC-Cu, Cu peaks disappear and no S peaks can be seen but some new peaks belonging to Cu-polysulfides CuS_x (marked with squares) appear.[37,38] The XRD results demonstrate the occurrence of chemical bonds between Cu and S in the HSMC-Cu-S, which indicates that the S is not only physically encapsulating in the nanoscale pores of carbon matrix, but also chemically interacting with Cu nanoparticles of the as-synthesized HSMC-Cu matrix. The S content of HSMC-Cu-S was measured using thermogravimetric analysis (TGA). Different from the evaporation of pure S in a temperature range of 180 to 300 °C (see Figure S1, Supporting Information), the S releasing from the HSMC-Cu-S composite takes place at much higher temperature. The HSMC-Cu-S starts to release S at about 250 °C and all of S (≈50%) can be extracted until the temperature reaches upon to 500 °C. The delay in extraction of S from the HSMC-Cu-S composite confirms that S is indeed stabilized by Cu nanoparticles in the HSMC-Cu-S composite. The high-temperature S-loss curve was similar to that reported in polymer-S composite synthesized by chemical reaction between polyacrylonitrile and S,[39–41] which is attributed to strong chemical bonding between S and the matrix.

The scanning electron microscopy (SEM) images of the HSMC and HSMC-Cu-S composite are presented in **Figure 2**. The surface morphology of the HSMC shows a spherical shape with a particle size of about 500 nm (Figure 2a). After depositing with Cu and S, no change in the morphology can be observed from the SEM images (Figure 2b), which indicates that the HSMC is a structural stable matrix supporting Cu and S. In addition, no large bulk S aggregations can be found in the composite from the SEM images of the HSMC-Cu-S. The EDS elemental maps for the HSMC-Cu-S composite shows that either Cu map or S map coincides well with that of C (Figure S2, Supporting Information), suggesting that both Cu and S are uniformly dispersed in the HSMC-Cu-S. The microstructures of the HSMC-Cu and HSMC-Cu-S were further characterized by high resolution transmission electron microscopy (HRTEM) and SAED and also shown in Figure 2. From Figure 2c, one can see that Cu nanoparticles with size ranged from 1 to 6 nm are uniformly distributed in HSMC matrix. The lattice of Cu can be clearly observed in HRTEM image and confirmed by the SAED pattern inserted. After S impregnation, it seems that the particle size becomes slightly larger as compared with that of nano-Cu particle in the HSMC-Cu (see Figure 2f); meanwhile, the SAED pattern of HSMC-Cu-S sample shows the clear rings made up of discrete spots, which should be related to the formation of Cu-polysulfides CuS_x.

To further confirm the interaction between Cu and S, the HSMC-Cu-S composite was characterized by X-ray photoelectron spectroscopy (XPS). **Figure 3** shows the survey scan and Cu 2p and S 2p binding energy spectra of the HSMC-Cu-S composite. The high-resolution Cu 2p spectrum shows four distinct peaks at around 932.7 and 952.5 eV for Cu^{1+} 2p3/2 and 2p1/2 core levels, and 934.8 and 954.3 eV for Cu^{2+} 2p3/2 and 2p1/2 core levels, revealing mixture valence states of Cu^{+1} and Cu^{+2} in the HSMC-Cu-S composite. Additionally, "shake-up" satellites at ≈945 and ≈965 eV for the Cu 2p3/2 and 2p1/2 core levels are clearly visible, which provide an evidence of an open $3d^9$ shell of Cu(+2).[42,43] The S 2p spectrum has three major peaks. The dual peaks positioned at 165.3 and 164.1 eV are assigned to S 2p1/2 and 2p3/2 due to spin orbit coupling, but the binding energies are slightly higher than those of the characteristic peaks of elemental S, indicating that the sulfur signal comes from the polysulfides CuS_x. The broad higher binding energy peak centered between 167 and 172 eV is also observed, which suggests the strong interaction between sulfur and copper.[44,45] The XPS results verify the formation of Cu-polysulfides CuS_x.

Specific surface area, pore size distribution, and pore volume of HSMC, HSMC-Cu and HSMC-Cu-S were measured using the N_2 adsorption-desorption isotherms, as shown in Figure S3 (Supporting Information). The HSMC shows an isotherm of typical type I, with pore sizes (see the inset in Figure S3, Supporting Information) in the range of approximately 3–6 nm and 10–12 nm. After loading with Cu and S, the N_2 sorption isotherms of both HSMC-Cu and HSMC-Cu-S still maintains type I, but the amount of the total adsorbed N_2 and the pore

© 2014 WILEY-VCH Verlag GmbH & Co. KGaA, Weinheim

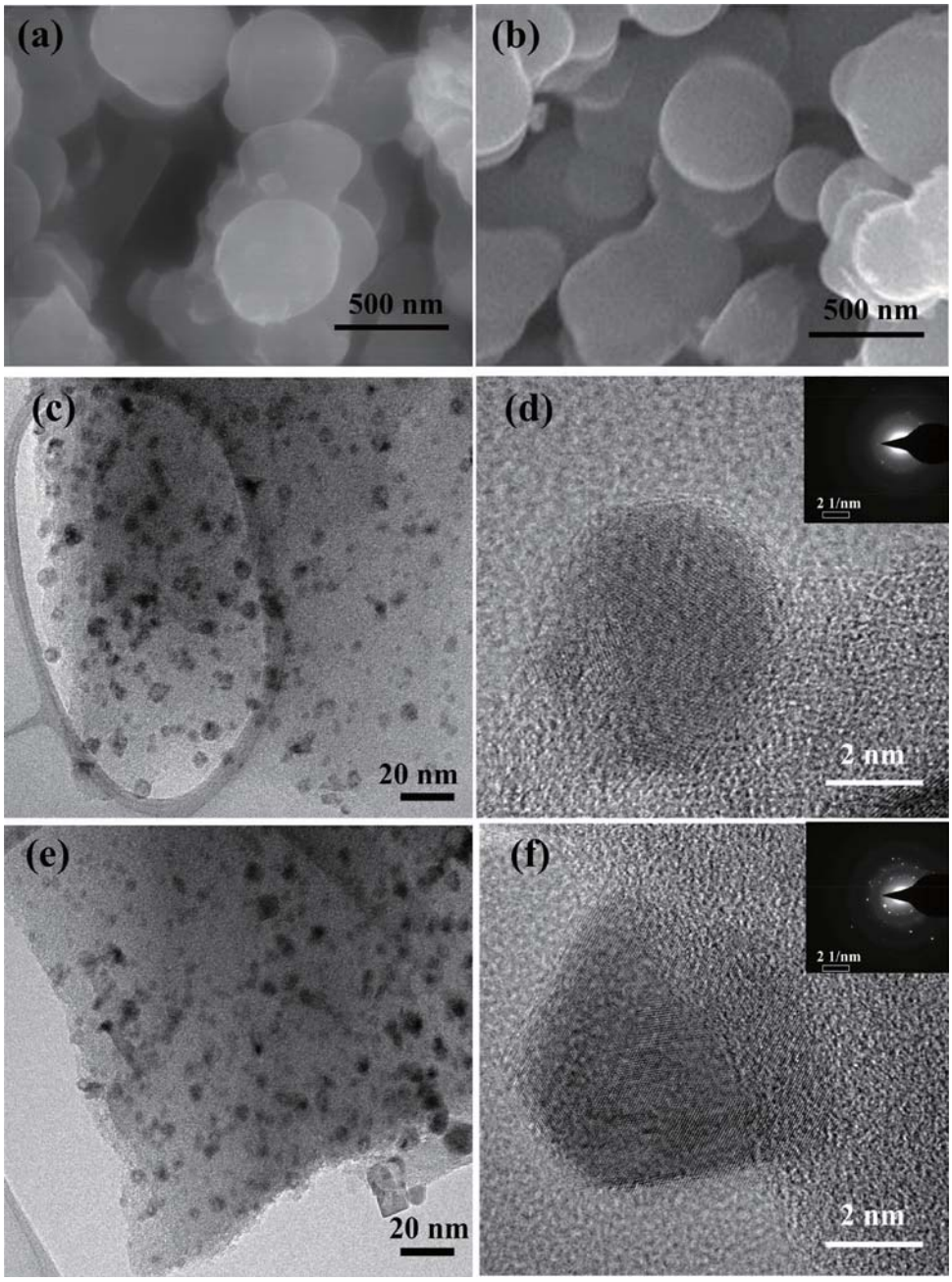

Figure 2. a) SEM image of the HSMC, b) SEM image of HSMC-Cu-S, c,d) HRTEM images and SAED image of the HSMC-Cu. e,f) HRTEM images and SAED image of the HSMC-Cu-S.

size were decreased. The HSMC possesses a high BET specific surface area of 1,780 m^2 g^{-1}, along with a total pore volume of 0.4 cm^3 g^{-1}. As the HSMC was filled with Cu, the BET specific surface area is reduced to around 1650 m^2 g^{-1} and the remaining portions of the pore volume are 85% of their total pore volume, i.e., there is a lot of space for subsequently loading S into the HSMC-Cu host. The HSMC-Cu-S composite fabricated via the S-solution-impregnation method has a BET specific surface area of approximately 100 m^2 g^{-1} and the pore volume of around 0.1 cm^3 g^{-1}, which still leaves room for volume changes of S/polysulfides during charge and discharge in the Na-S battery.

The electrochemical performance of the HSMC-Cu-S composite was investigated as a cathode for Na-ion batteries in coin cells. The initial three cycle sodiation/desodiation behaviors of the HSMC-Cu-S electrodes were characterized using cyclic voltammetry (CV), shown in **Figure 4**a. During the catholic scan (sodiation), the cell exhibits a very weak peak at about 2.1–2.2 V (vs. Na/Na^+) along with a strong peak centered at around 0.8 V (vs. Na/Na^+) in the first cycle. The faint peak at high voltage is associated to the formation of soluble high-order polysulfides through the reaction of $S_8 + Na \rightarrow Na_2S_n$ ($n > 4$) due to the existence of minor S_8 in the composite,[46] while the cathodic

© 2014 WILEY-VCH Verlag GmbH & Co. KGaA, Weinheim

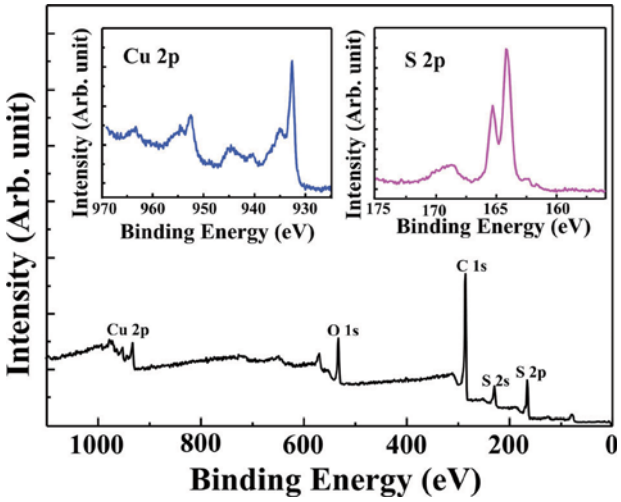

Figure 3. High-resolution XPS spectra of HSMC-Cu-S composite, with insets showing the Cu 2p and S 2p spectra.

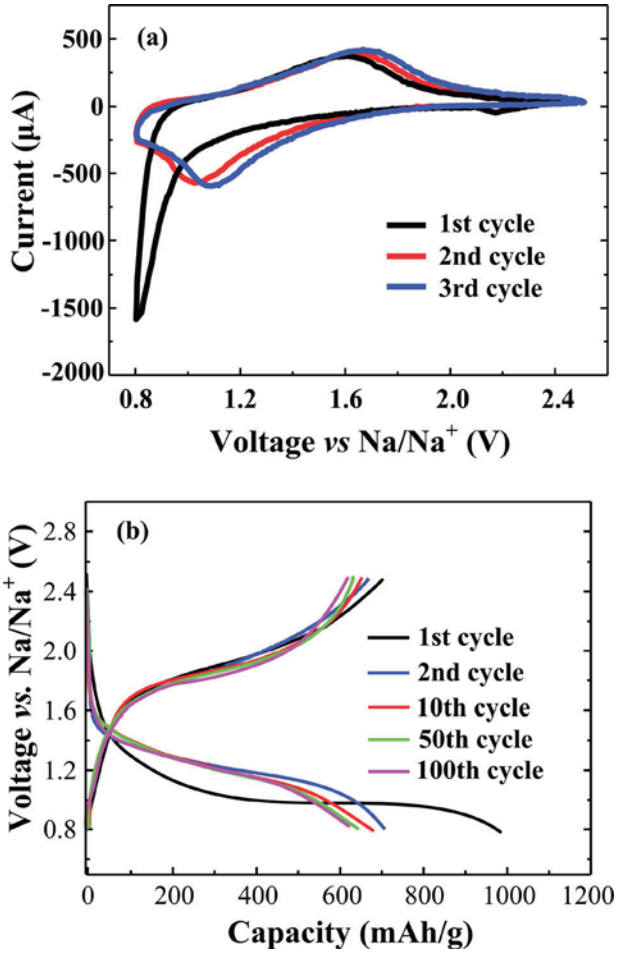

Figure 4. a) Cyclic voltammograms of the HSMC-Cu-S composite cathode in RT Na-S cell in the initial three cycles within the voltage window of 0.8–2.5 V at a scan rate of 0.1 mV s^{-1}. b) Discharge/charge voltage profiles of the HSMC-Cu-S composite cathode in RT Na-S cell during the 1st, 2nd, 10th, 50th and 100th cycle.

peak near 0.8 V (vs. Na/Na^+) corresponds to the sodiation of the chemical bonding S. After the first cycle, the weak cathodic peak vanishes in the second cycle, suggesting that high-order polysulfides formed from reaction between the S_8 and Na were totally dissolved into the electrolyte; moreover, the low-voltage peak current was reduced and shifted in the more positive direction due to the introduction of large defects in the electrode and pore size expansion of carbon in the first sodiation.[47–50] For the anodic scan, only one peak at 1.6 V (vs. Na/Na^+), was observed, which is associated with the oxidation of Na_2S. The stable cathodic and anodic current peaks in the first and following scans also demonstrate good cycling stability of the HSMC-Cu-S composite cathode. Figure 4b shows the discharge/charge voltage profiles in the 1st, 2nd, 10th, 50th and 100th cycle at a current rate of 0.03C (1C = 1,675 mA g^{-1}). The HSMC-Cu-S cathode shows a very short slope at relatively high voltage range (≥1.6 V) following with a long plateau at low voltage (≈1.1 V) in the first discharge and only a plateau in the charge in the Na-S cell, and in the second discharge, the short high-voltage slope almost vanishes and only one long plateau can be observed. Such a phenomenon of only one charging and discharging plateau was previously reported both in carbon-S composite cathodes and in conductive polymer-S composite cathodes synthesized at relatively higher temperature (≥300 °C) and was attributed to chemical interaction between S and the matrix.[21,41,46] Therefore, the one discharge/charge plateau feature for the HSMC-Cu-S cathode in the Na-S cell should be mainly ascribed to the S stabilized by Cu nanoparticle through strong interaction between Cu and S. In addition, the disappearance of the short high-voltage slope in the second discharge is due to the dissolution of high-order polysulfide intermediates and the side reaction between dissolved polysulfide anions and carbonate solvent. The lithiation capacity is around 1000 mAh g^{-1} in the first cycle, 710 mAh g^{-1} in the second cycle, and retains approximately 610 mAh g^{-1} for 110 cycles, showing fairly stable cycle life. The irreversible capacity of about 290 mAh g^{-1} in the first charge/discharge cycle is due to dissolution of high-order polysulfide intermediates and the side reaction between dissolved polysulfide anions and carbonate solvent, which coincides with the above CV scan result. The reversible capacity is much higher than the conventional HT Na-S batteries.[3,4] These results suggest that high utilization of S occurred in this work due to the high conductivity of the HSMC-Cu matrix and Cu nanoparticles chemical stabilization of S. Although the S loading reached up to 50%, in consideration of the possible contributions of other components (e.g., HSMC-Cu and carbon black) to the performance of the HSMC-Cu-S electrode, we conducted a control experiment using HSMC-Cu as a cathode, that is, a HSMC-Cu electrode without S was prepared and tested in RT Na-S cell identical to the fabrication procedure and electrochemical measurements of the HSMC-Cu-S electrode. The initial discharge capacity of the HSMC-Cu electrode in the Na-S cell was around 200 mAh g^{-1}. After the first cycle, the capacity quickly dropped to around 50 mAh g^{-1} in the second cycle and gradually declined with progressive cycling (the results shown in Figure S4, Supporting Information). Obviously, the effects of other components on the electrochemical properties of the HSMC-Cu-S electrode are negligible, which indicates that the Cu nanoparticles chemical

© 2014 WILEY-VCH Verlag GmbH & Co. KGaA, Weinheim

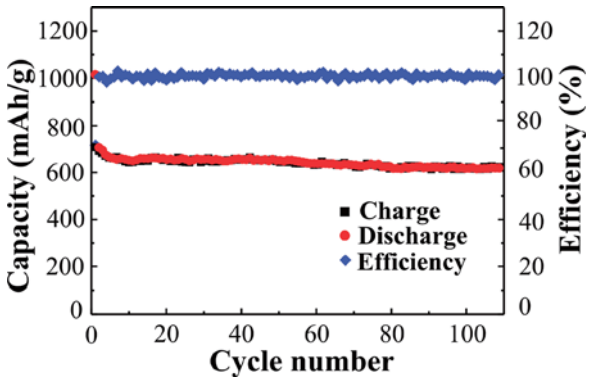

Figure 5. Cycling performance and Coulombic efficiency of the HSMC-Cu-S composite cathode in RT Na-S cell.

stabilization of S is responsible for the high reversible capacity of the HSMC-Cu-S cathode in the RT Na-S battery.

The cycling stability of the HSMC-Cu-S electrode at 0.03C is presented in **Figure 5**, showing high Coulombic efficiency and long cycling stability. The desodiation capacity maintains around 610 mAh g^{-1} after 110 cycles, which corresponds to 86% of that in the second cycle. Additionally, the Coulumbic efficiency at the 0.03C rate closes to 100% over 110 cycles except the first cycle. This reveals that the dissolution and shuttle effects were completely prevented, indicating that the strong interaction between Cu and S and the high electronic conductivity of Cu largely increase the S utilization, even when S loading reaches to 50%, and effectively improve the cycling stability of the S cathode in the liquid electrolyte. Identical to the HSMC-Cu-S composite preparation procedure, a sample with 50% of S directly impregnating into the pristine HSMC (denoted as HSMC-S) was also prepared as a control sample and its electrochemical performance was investigated as a cathode for Na-ion batteries in coin cells. The initial discharge capacity of the HSMC-S cathode is around 550 mAh g^{-1} in Na-S cell at 0.03C, far less than the value of the HSMC-Cu-S cathode; after the initial few cycles, the capacities drop to less than 100 mAh g^{-1} (see Figure S5, Supporting Information). The low capacity is not surprising because of dissolution of high-order polysulfide intermediates (Na_2S_x, $4 \le x \le 8$) in liquid organic electrolytes and the side reaction between dissolved polysulfide anions and carbonate solvent of the electrolytes. This fully proves that Cu nanoparticles chemical stabilization of S is responsible for the exceptional performance of the HSMC-Cu-S cathode in the RT Na-S battery.

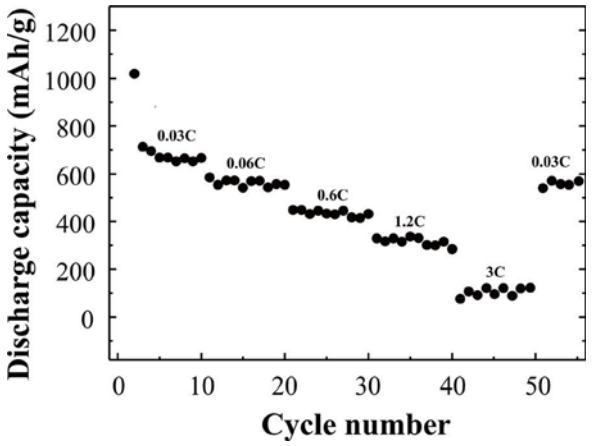

Figure 6. Rate performance of the HSMC-Cu-S composite cathode at different current rate from 0.03 to 3C.

The rate capability was also checked at different rates from 0.03C to 3C, displaying in **Figure 6**. A capacity of about 350 mAh g^{-1} was delivered at a high rate of 1.2C. Even when increasing the rate up to 3C, a capacity of more than 100 mAh g^{-1} can still be obtained. Most of all, one can see from the rate capability profiles that the capacity of approximately 580 mAh g^{-1} can be reached again after 40 cycles when the rate is returned from 3C to 0.03C, thereby demonstrating great merit for an abuse tolerance of Na-S battery with varied current rates. Simply dispersing 10% of Cu throughout HSMC can also enhance the rate performance of S-based cathode with 50% content, which is related to the highly conductive HSMC-Cu matrix.

Overall, the HSMC-Cu-S cathodes show stable, high and reversible capacities together with good rate and cycling capabilities in the RT Na-S batteries. The Cu nano-inclusions play the key roles on the exceptional electrochemical performance of HSMC-Cu-S composite cathode in the RT Na-S battery. As the Cu is deposited into HSMC, the Cu nanoparticles percolate throughout HSMC host and then chemically stabilize S to form Cu polysulfide clusters as loading S. These Cu nano-inclusions enhance the electronic conductivity of HSMC-Cu-S cathodes. By combining with inherent mesoporous structure of HSMC, nano-Cu particles decorated the HSMC material and provide superior confinement ability for S and polysulfides, a sufficient space to accommodate S volumetric expansion, a large contact area with the S, and a short transport pathway for both electrons and Na^+, thus resulting in effective stabilization of the S cathode with high S loading in liquid electrolyte and significantly increasing its utilization. Finally, this demonstrates excellent electrochemical performance of the S-based cathode in the RT Na-S batteries.

In summary, a small amount (10%) of Cu nanoparticle loading in HSMC can effectively stabilize the 50% S loaded in HSMC-Cu-S cathode for the RT Na-S battery. The unique structural HSMC-Cu-S composite cathode shows a Coulumbic efficiency of 100%, maintains capacities of around 610 mAh g^{-1} at a 0.03C rate with progressive cycling up to 110 cycles, and provides a capacity of 100 mAh g^{-1} even at a high rate of 3C. The exceptional performance of HSMC-Cu-S cathode is due to the synergistical effects of the Cu nano-inclusions and the HSMC host as: i) the nano-Cu particles immobilize S by formation of solid Cu polysulfide clusters through strong interaction between Cu and S; ii) these Cu nano-inclusions enhance the electronic conductivity of carbon-S cathodes; and iii) the HSMC host provides free space for volume change of S/polysulfides during charging/discharging. The results represent that small amount of metal nanoparticle anchored in HSMC can substantially stabilize the S cathode and lead to the improvements of the cycling stability and rate capability.

© 2014 WILEY-VCH Verlag GmbH & Co. KGaA, Weinheim

Experimental Section

Preparation of HSMC-Cu-S Nanocomposites: A commercial high-surface-area mesoporous carbon (HSMC) was purchased from ACS Material LLC, USA and used as received. Copper dinitrate ($Cu(NO_3)_2$, Sigma-Aldrich, 98%) was first dissolved in ethanol alcohol (Aldrich 98%) to form a 50% $Cu(NO_3)_2$ content solution ($Cu(NO_3)_2$/EtOH-solution). An ultrasonic-assisted multiple wetness impregnation and synchro-dry method was applied to load copper dinitrate in the HSMC, i.e., the copper dinitrate solution was first added to the HSMC and subsequently sonicated with a Branson Sonifier S-450A at 60 °C to evaporate the solvent. This process was repeated until a certain amount of $Cu(NO_3)_2$ was added to the HSMC. The resulting sample was then reduced at 200 °C for 1 h with a heating rate of 5 °C min^{-1} under argon mixed with 5% hydrogen environment. The HSMC-Cu with different content of Cu can be prepared by adjusting the amount of $Cu(NO_3)_2$ addition. Experiments that have not yet been published found that the HSMC deposited with 10% Cu has the best comprehensive electrochemical performances of S cathode in Na-S batteries among 5, 15 and 20% Cu. Therefore, the HSMC-Cu material with 10% Cu was synthesized and used in this experiment. The HSMC-Cu-S nanocomposite was prepared through a simple solution-impregnation strategy: sulfur (Sigma-Aldrich, 99.5%) was first dissolved in carbon disulfide (CS_2, Aldrich 98%) to form a 50% sulfur content solution (S/CS_2-solution), 1 g as-synthesized HSMC-Cu powder was added to 2 g of the S/CS_2 solution. To effectively load S into HSMC, the ultrasonic-assisted multiple wetness impregnation and synchro-dry technique was also employed. The resulting sample was dried at 60 °C in a vacuum for 24 h, and around 50% of S was loaded into the as-prepared composite. Identical to the HSMC-Cu-S composite preparation procedure, a sample with 50% of S direct-impregnating into the pristine HSMC was also prepared (denoted as HSMC-S hereafter) as a control sample. To obtain the actual sulfur content in the sulfur-containing samples, TGA was performed on a Netzsch STA 409 PC, Germany, with a heating rate of 10 °C/min, and highly pure Ar as the purge gas.

Structural Characterization: XRD patterns were recorded on Rigaku D/max 2400, Japan, with Cu Kα radiation in the 2-Theta range from 10–80°. BET specific surface area and pore size and volume were analyzed using N_2 adsorption–desorption isotherm at 77 K on ASAP2020 (Micromeritics Instrument Corp., USA). SEM images were obtained on a Hitachi S-4700, Japan, operating at 15 kV and equipped with an EDS. The TEM samples were examined in a JEM 3010 microscope. High spatial resolution imaging and microanalysis were performed with an FEI Titan 80–300 analytical scanning transmission electron microscope (STEM) operated at 300 kV accelerating voltage and equipped with a Fischione Instruments model 3000 high-angle annular dark-field (HAADF) detector and an EDAX lithium-drifted silicon X-ray energy-dispersive spectrometer (XEDS). XPS)data were collected at room temperature with a Kratos Analytical spectrometer and monochromatic Al Kα (1486.6 eV) X-ray source.

Electrochemical Measurements: The S-containing composite was mixed with acetylene black and sodium carboxymethyl cellulose binder in a weight ratio of 80:10:10, with distilled water as a dispersant. The slurry was coated on an aluminum foil to obtain a film with approximately 80 μm thickness and dried in a vacuum oven at 100 °C overnight. The active material loading was around 1 mg cm^{-2}. Na-ion batteries were assembled with sodium as the counter electrode, 1.0 M $NaClO_4$ in a mixture of ethylene carbonate/dimethyl carbonate (EC/DMC, 1:1 by volume) as the electrolyte, and Celgard 3501 (Celgard, LLC Corp., USA) as the separator. The charge and discharge performances of the Na-S batteries were tested with using LAND CT2001A battery test instrument (LAND Electronic Co., China) and potential ranges were controlled between 0.8 and 2.5 V (vs. Na/Na^+) at ambient temperature. The specific capacity was calculated on the basis of the active sulfur material obtained from TGA measurement. The cyclic voltammetry (CV) measurement was conducted with a Gamry Reference 3000 (Gamry Co., USA) at a scan rate of 0.1 mV s^{-1}.

Supporting Information

Supporting Information is available from the Wiley Online Library or from the author.

Acknowledgements

The authors gratefully acknowledge the support of the National Science Foundation of China (No. 51272157). The authors would like to thank Prof. Chunsheng Wang of the University of Maryland (USA) for constructive suggestions, and Dr. Feng Yi and Dr. Zhipeng Li of National Institute of Standards and Technology for their kind help with the TGA and TEM measurements.

Received: February 6, 2014
Revised: March 1, 2014
Published online:

[1] M. Winter, J. B. Brodd, *Chem. Rev.* **2004**, *104*, 4245.
[2] B. Dunn, H. Kamath, J. M. Tarascon, *Science* **2011**, *334*, 928.
[3] Z. Yang, J. Zhang, M. Kintner-Meyer, X. Lu, D. Choi, J. P. Lemmon, J. Liu, *Chem. Rev.* **2011**, *111*, 3577.
[4] X. Lu, G. Xia, J. P. Lemmon, Z. Yang, *J. Power Souces* **2010**, *195*, 2431.
[5] X. Lu, B. W. Kirby, W. Xu, G. Li, J. Y. Kim, J. P. Lemmon, V. L. Sprenkle, Z. Yang, *Energy Environ. Sci.* **2013**, *6*, 299.
[6] C. W. Park, J. H. Ahn, H. S. Ryu, K. W. Kim, H. J. Ahn, *Electrochem. Solid-State Lett.* **2006**, *9*, A123.
[7] H. Ryu, T. Kim, K. Kim, J. H. Ahn, T. Nam, G. Wang, H. J. Ahn, *J. Power Sources* **2011**, *196*, 5186.
[8] D. Kumar, M. Suleman, S. A. Hashmi, *Solid State Ionics* **2011**, *202*, 45.
[9] K. Xu, *Chem. Rev.* **2004**, *104*, 4303.
[10] Y. Jung, S. Kim, *Electrochem. Commun.* **2007**, *9*, 249.
[11] S. S. Zhang, *Energies* **2012**, *5*, 5190.
[12] L. Suo, Y. Hu, H. Li, M. Armand, L. Chen, *Nat. Commun.* **2013**, *4*, 1481.
[13] X. Ji, L. F. Nazar, *J. Mater. Chem.* **2010**, *20*, 9821.
[14] A. Manthiram, Y. Fu, Y. Su, *Acc. Chem. Res.* **2013**, *46*, 1051.
[15] C. Barchasz, F. Molton, C. Duboc, J. Lepretre, S. Patoux, F. Alloin, *Anal. Chem.* **2012**, *84*, 3973.
[16] Y. Diao, K. Xie, S. Xiong, X. Hong, *J. Electrochem. Soc.* **2012**, *159*, A421.
[17] Y. V. Mikhaylik, J. R. Akridge, *J. Electrochem. Soc.* **2004**, *151*, A1969.
[18] Y. Yang, G. Zheng, Y. Cui, *Chem. Soc. Rev.* **2013**, *42*, 3018.
[19] M. Song, E. J. Cairns, Y. Zhang, *Nanoscale* **2013**, *5*, 2186.
[20] X. Ji, K. T. Lee, L. F. Nazar, *Nat. Mater.* **2009**, *8*, 500.
[21] B. Zhang, X. Qin, G. Li, X. Gao, *Energy Environ. Sci.* **2010**, *3*, 1531.
[22] L. Ji, M. Rao, S. Aloni, L. Wang, E. J. Cairns, Y. Zhang, *Energy Environ. Sci.* **2011**, *4*, 5053.
[23] N. Jayaprakash, J. Shen, S. S. Moganty, A. Corona, L. A. Archer, *Angew. Chem. Int. Ed.* **2011**, *50*, 5904.
[24] W. Weng, V. G. Pol, K. Amine, *Adv. Mater.* **2013**, *25*, 1608.
[25] J. Guo, Y. Xu, C. Wang, *Nano Lett.* **2011**, *11*, 4288.
[26] L. Ji, M. Rao, H. Zheng, L. Zhang, Y. Li, W. Duan, J. Guo, E. J. Cairns, Y. Zhang, *J. Am. Chem. Soc.* **2011**, *133*, 18522.
[27] L. Zhang, L. Ji, P. Glans, Y. Zhang, J. Zhu, J. Guo, *Phys. Chem. Chem. Phys.* **2012**, *14*, 13670.
[28] G. He, X. Ji, L. F. Nazar, *Energy Environ. Sci.* **2011**, *4*, 2878.
[29] S. Zhang, J. A. Read, *J. Power Sources* **2012**, *200*, 77.
[30] J. Guo, Z. Yang, Y. Yu, H. D. Abruna, L. A. Archer, *J. Am. Chem. Soc.* **2013**, *135*, 763.

© 2014 WILEY-VCH Verlag GmbH & Co. KGaA, Weinheim

[31] Y. Wang, J. Wu, Y. Tang, X. Lu, C. Yang, M. Qin, F. Huang, X. Li, X. Zhang, *ACS Appl. Mater. Interfaces* **2012**, *4*, 4246.
[32] S. Han, H. Kim, M. Song, P. S. Lee, J. Lee, H. Ahn, *J. Alloys Compd.* **2003**, *349*, 290.
[33] Y. Wang, X. Zhang, P. Chen, H. Liao, S. Cheng, *Electrochim. Acta* **2012**, *80*, 264.
[34] A. Sakuda, N. Taguchi, T. Takeuchi, H. Koyayashi, H. Sakaebe, K. Tatsumi, Z. Ogumi, *Electrochem. Commun.* **2013**, *31*, 71.
[35] R. Cai, J. Chen, J. Zhu, C. Xu, W. Zhang, C. Zhang, W. Shi, H. Tan, D. Yang, H. H. Hng, T. M. Lim, Q. Yan, *J. Phys. Chem. C* **2012**, *116*, 12468.
[36] Y. Du, Z. Yin, J. Zhu, X. Huang, X. Wu, Z. Zeng, Q. Yan, H. Zhang, *Nat. Commun.* **2013**, *3*, 1177.
[37] R. Steudel, *Elemental Sulfur and Sulfur-Rich Compounds II*, Springer-Verlag, Berlin Heidelberg New York **2003**.
[38] H. Wei, Z. Ye, M. Li, Y. Su, Z. Yang, Y. Zhang, *CrystEngComm* **2011**, *13*, 2222.
[39] J. Fanous, M. Wegner, J. Grimminger, A. Andresen, M. R. Buchmeiser, *Chem. Mater.* **2011**, *23*, 5024.
[40] M. Sun, S. Zhang, T. Jiang, L. Zhang, J. Yu, *Electrochem. Commun.* **2008**, *10*, 1819.
[41] J. Wang, J. Yang, J. Xie, N. Xu, *Adv. Mater.* **2002**, *14*, 963.
[42] C. Chusuei, M. Brookshier, D. Goodman, *Langmuir* **1999**, *15*, 2806.
[43] V. Krylova, M. Andrulevicius, *Int. J. Photoenergy* **2009**, DOI: 10.1155/2009/304308.
[44] V. Toniazzo, C. Mustin, J. Portal, B. Humbert, R. Benoit, R. Erre, *Appl. Surf. Sci.* **1999**, *143*, 229.
[45] G. Greczynski, Th. Kugler, W. Salaneck, *Thin Solid Film* **1999**, *354*, 129.
[46] S. Zheng, Y. Chen, Y. Xu, F. Yi, Y. Zhu, Y. Liu, J. Yang, C. Wang, *ACS Nano* **2013**, *7*, 10995.
[47] U. Kasavajjula, C. Wang, A. J. Appleby, *J. Power Sources* **2007**, *163*, 1003.
[48] J. Guo, Q. Liu, C. Wang, M. R. Zachariah, *Adv. Funct. Mater.* **2012**, *22*, 803.
[49] Y. Zhu, X. Han, Y. Xu, Y. Liu, S. Zheng, K. Xu, L. Hu, C. Wang, *ACS Nano* **2013**, *7*, 6378.
[50] C. Luo, Y. Xu, Y. Zhu, Y. Liu, S. Zheng, Y. Liu, A. Langrock, C. Wang, *ACS Nano* **2013**, *9*, 8003

 © 2014 WILEY-VCH Verlag GmbH & Co. KGaA, Weinheim